Heliyon 11 (2025) e42693

Contents lists available at ScienceDirect

Heliyon

journal homepage: www.cell.com/heliyon

Research article

Inhibitory effects of saffron compounds on multiple sclerosis: Molecular docking and dynamic, enhancing properties with gold nanoparticles and evaluating antioxidant, antibacterial, cytotoxicity

Shaghayegh Mohammadi [a], Hamed Farjam [a], Sharieh Hosseini [b,*], Kambiz Larijani [a]

[a] Department of Chemistry, Science and Research Branch, Islamic Azad University, Tehran, Iran
[b] Department of Chemistry, Faculty of Pharmaceutical Chemistry, Tehran Medical Sciences, Islamic Azad University, Tehran, Iran

ARTICLE INFO

Keywords:
Saffron
Gold nanoparticle
Multiple sclerosis
Molecular docking
MTT assay
Antibacterial

ABSTRACT

The unique properties of nanoparticles, such as their small size and the ability to cross the blood-brain barrier, make them well-suited for targeted drug delivery to the central nervous system. Ongoing research is dedicated to developing innovative nanoparticle-based therapies for a neurological disorder; multiple sclerosis (MS). The study confirmed green synthesis as the optimal method for producing environmentally friendly compounds. The nanoparticles were characterized by Fourier transform infrared spectroscopy (FT-IR), X-ray powder diffraction (XRD), and transmission electron microscopy (TEM). To evaluate the antioxidant properties, we employed the 2,2-diphenyl-1-picrylhydrazyl (DPPH) method, while conducting a comprehensive examination of antibacterial activity against both Gram-negative (*E. coli*) and Gram-positive bacteria (*S. aureus*). Moreover, we performed a thorough assessment of cellular toxicity using saffron extracts and nanoparticles on C6 and SH-SY5Y cells. We employed molecular docking computational methods to investigate the potential inhibitory effects of natural compounds derived from saffron on Multiple Sclerosis. The results of biological activities and computational modeling show that gold nanoparticles improve the performance of plant compounds and also these compounds can be involved in inhibiting proteins responsible for multiple sclerosis.

1. Introduction

The crocus plant bears violet-colored flowers, the stigmas of which are used as a spice [1]. Crocin, safranal, and picrocrocin are the main bioactive ingredients of saffron responsible for the color, aroma, and bitterness of the spice, respectively [2]. Oxidative stress, defined as a disturbance in the balance between the production of reactive oxygen species (free radicals) and antioxidant defenses, is implicated in several diseases, such as cancer, heart and vascular diseases, obesity, diabetes mellitus, and neurodegenerative disorders (i.e. Alzheimer's, Parkinson's, Huntington's and multiple sclerosis) [3]. All medicinal effects of saffron are surely related to its strong antioxidant activity, which is ascribed to crocin, crocetin, and safranal compounds [4]. Saffron use as an antioxidant source prevents demyelination and reduces symptoms in multiple sclerosis [3,5]. Crocin protects against neuroinflammatory conditions that were inducted in brain cells due to endoplasmic reticulum stress. Furthermore, in PC-12 cells, crocin was found to reduce the effect of TNF-a

* Corresponding author.
E-mail address: Shariehosseini@yahoo.com (S. Hosseini).

https://doi.org/10.1016/j.heliyon.2025.e42693
Received 26 July 2024; Received in revised form 12 February 2025; Accepted 12 February 2025
Available online 15 February 2025

along with Bcl-XS and LICE mRNAs expressions and improved the cytokine-induced reduction in expression of Bcl-XL mRNA in experimented brain microglial cells [6,7]. Saffron petals contain several essential anti-inflammatory chemical compounds, including gallic acid, chlorogenic acid, epigallocatechin gallate (ECGC), isoquercetin, and kaempferol. These compounds have been recognized for their potential to reduce inflammation and provide health benefits. Predominantly found in the reddish-orange stigmas of the saffron plant are compounds such as crocin, crocetin, picrocrocin, safranal, linolenic acid, and HTCC. These compounds contribute to the distinct aroma, flavor, and color of saffron, and they have also been investigated for their potential health benefits and therapeutic properties [8,9] (see Fig. 7).

During the last decade, there has been growing concern to use biological substances particularly flora to synthesize nanomaterials. The biological synthesis of nanomaterials involving different plant is gaining worldwide attention because of their benign approach. There is a great concern to search for environmentally friendly methods, which results in the development of bio-nanotechnology [10, 11]. This eco-friendly procedure for the synthesis of nanoparticles neither involves very harmful chemicals nor harsh reaction conditions [12,13]. The green synthesis of AuNPs is a simple, safe, dynamic, and facile process as its protocol follows a moderate environment without extreme temperatures or pressures. Green synthesized AuNPs application improves the diagnosis and treatment of many human diseases [14]. To synthesize stable nanoparticles, gold (Au) is regarded as a suitable metal [15–17]. The green synthesis of gold nanoparticles has been reported using plant tissues, bacteria, fungi, actinomycetes, etc [18]. However, the green synthesis of AuNPs from the plant is an eco-friendly approach. In the biosynthesis of AuNPs from the plant, different plant parts [18,19]. Plant extracts contain various metabolites or organic compounds such as alkaloids, flavonoids, proteins, polysaccharides, cellulose, and phenolic compounds, which are utilized for nanoparticle synthesis. The variation in composition and concentration of reducing agents in plant extracts is responsible for different sizes, shapes, and morphological nanoparticle synthesis [20]. Researchers have reported that the size and morphology of nanoparticles can be expected to be different by changing the synthesis parameters, including pH, metal salt, temperature, and reaction time [21].

Multiple sclerosis (MS) is the most common non-traumatic disabling disease to affects young adults [22]. MS is a complex disease; many genes modestly increase disease susceptibility in addition to several well-defined environmental factors, in particular vitamin D or ultraviolet B light (UVB) exposure, Epstein–Barr virus (EBV)infection, obesity, and smoking [23]. Multiple sclerosis has historically been classified as an organ-specific T-cell-mediated autoimmune disease. However, the success of B-cell targeted therapies challenges the standard T-cell autoimmune dogma [24]. It is traditionally viewed as a two-stage disease, with early inflammation responsible for relapsing-remitting disease and delayed neurodegeneration causing non-relapsing progression, i.e. secondary and primary progressive MS [25,26]. Tumor necrosis factor-α (TNF-α), is a principal mediator of the inflammatory response and may be important in the pathogenesis and progression of multiple sclerosis, an inflammatory disease of the central nervous system [27]. MMP-9 facilitates the migration of T cells to the central nervous system, leading to increased inflammation [28,29].

Lymphocryptovirus is a genus of dsDNA viruses in the Herpesviridae family that infect many mammals, including humans. Human herpesvirus 4 (formerly called Epstein-Barr virus (EBV)) is responsible for mononucleosis in humans. Two viral proteins, nuclear antigen Epstein-Barr virus (EBNA) and latent membrane protein (LMP), assume multifunctional roles in genome maintenance, replication, and segregation. The hidden membrane protein, on the other hand, acts as the primary viral oncoprotein under investigation for potential therapeutic targeting. Structurally, this protein exhibits signaling motifs similar to tumor necrosis factor, making it a significant target for potential therapeutic interventions [30,31]. Typically, this virus is transmitted through saliva exchange, although transmission via organ transplantation and potentially sexual contact is also possible [32]. EBNA1 is responsible for the origin of replication (oriP) dependent replication and maintenance of viral episomes during latent infection [33,34] and EBNA1 dimer interacts with the DS (dyad symmetry) element within the origin of replication oriP and with a host mitotic chromosome to initiate viral DNA replication during latency [33,35,36]. and LMP1 acts as a CD40 functional homolog to prevent apoptosis of infected B-lymphocytes and drive their proliferation.

2. Material and methods

2.1. Nanoparticle synthesis

The initial phase of nanoparticle synthesis involves the preparation of the plant extract. To obtain the extract, 10 g of saffron were immersed in 150 ml of deionized water. This mixture was then heated in a water bath at 80 °C for 40 min, with intermittent stirring. After cooling to room temperature, the solution underwent filtration.

Following this, 8 mL of a gold salt solution with a concentration of 0.001 M were combined with 2 ml of the saffron extract. Stirring for approximately 5 min ensued until the solution transitioned in color from yellow to a deep purple hue. To confirm nanoparticle formation, the sample was scanned in the wavelength range of 300–700 nm using an ultraviolet spectrophotometer. For FT-IR and XRD peak analysis, in addition to obtaining TEM images, the solution underwent centrifugation; the resulting precipitate was washed with deionized water, and the final precipitate was dissolved in deionized water. Then to examine stability, zeta potential and DLS for both fresh and one-year solutions were used.

2.2. Antioxidant properties investigation

For each of the plant extract and synthesized nanoparticle solutions, alongside ascorbic acid as standard, solutions with concentrations of 250, 125, 62.5, and 31.25 ppm were prepared in methanol. Additionally, a 40 ppm DPPH solution was created in methanol. In separate containers, 1 ml of each concentration of plant extract, nanoparticles, and standard solutions were combined. To each, 1 ml

of DPPH solution and 3 ml of methanol were added, and the mixtures were incubated for 40 min. After this incubation period, the absorption levels of each solution at a wavelength of 517 nm were analyzed using a UV–VIS spectrophotometer.

2.3. Antibacterial assessment

The antibacterial efficacy of the sample against both Gram-positive bacteria (*S. aureus*) and Gram-negative bacteria (*E. coli*) was evaluated using the Colony Forming Unit (CFU) method [37]. Initially, the samples underwent thorough sterilization, and a bacterial suspension was meticulously prepared, adhering to the 0.5 McFarland standard, with its optical density (OD) carefully verified at λ 630 nm.

Subsequently, 1000 μL of the bacterial suspension was introduced to the sterile samples, followed by a 24-h incubation at 37 ± 1 °C. Also, a control sample was considered for each bacteria for a more detailed investigation and the possibility of comparing the results, After this incubation period, dilution was carried out at a ratio of 1:10, and the resulting diluted bacteria were meticulously plated on a Nutrient Agar culture medium. The plates were then subjected to an 18-h incubation at a temperature of 37 ± 1 °C. The ImageJ program played a crucial role in quantifying the average number of colonies post-incubation, and the antibacterial effectiveness of the sample was expressed as a percentage using the following equation.

$$R\ (\%) = \frac{N_A - N_B}{N_A} \times 100 \tag{1}$$

Where R (%) is the Antibacterial property of the sample in percent, N_A is the Number of colonies in the sample before contact and N_B is the number of colonies in the sample after contact.

2.4. MTT assay

The MTT (3-[4,5-dimethylthiazol-2-yl]-2,5 diphenyl tetrazolium bromide) assay is based on the conversion of MTT into formazan crystals by living cells, which determines mitochondrial activity. Since for most cell populations, the total mitochondrial activity is related to the number of viable cells, this assay is broadly used to measure the in vitro cytotoxic effects of drugs on cell lines or primary patient cells [38]. We decided to choose SH-SY5Y and C6 cells, a human neuronal immortalized cell line and rat neuronal cell line respectively, because it is widely used in cell culture models for providing insight into neuronal biology and has been largely used for in vitro studies to investigate neuronal toxicity, apoptotic mechanisms, and neuroimmune signaling between astrocytes and neurons in many neurodegenerative diseases [38,39].

In this study, C6 cells (NCBI C575) and SH-SY5Y (NCBI C611) were utilized. Post-thawing, these cells were transferred to flasks containing DMEM + F12 for C6 cells and just DMEM for SH-SY5Y cells culture medium supplemented with 10 % FBS. The flasks were then incubated at 37 °C, 90 % humidity, and a 5 % carbon dioxide concentration. Notably, the culture medium underwent replacement every 3–4 days. Also, control samples were considered for each cells for a more detailed investigation and the possibility of comparing the results.

To assess sample toxicity and its impact on cell growth and proliferation, specific concentrations of the samples were prepared. For evaluating cell proliferation, 1.04×10^4 cells, along with 100 μL of culture medium, were added to each well of a 96-well cell culture plate. This plate was then incubated at 37 °C for 24 h to ensure cell adhesion to the plate's bottom. After confirming cell adhesion, the culture medium was mostly removed, and each well received 90 μL of the prepared concentrations, along with 10 μL of FBS. The cells were exposed to these concentrations for an additional 48 h.

Subsequently, the culture medium was aspirated, and 100 μL of MTT solution at a concentration of 0.5 mg/ml were added to each well. The plate underwent a 4-h incubation. Post-incubation, the solution was aspirated, and isopropanol was introduced to dissolve the purple crystals formed. To expedite the dissolution of MTT residues, the plate was placed on a shaker for 15 min. The concentration of the dissolved substance in isopropanol was then measured using a microplate reader (ELx 808, Bio Tek, USA) at a wavelength of 570 nm. Higher optical density (OD) in wells indicates greater cell density. Thus, wells with more cells can be identified using the following equation and compared with the control sample (DMEM + F12 culture medium containing 10 μL of FBS for C6 cells and DMEM culture medium containing 10 μL of FBS for SH-SY5Y cells).

$$\text{Toxicity}\% = \left(1 - \frac{mean\ OD\ of\ sample}{mean\ OD\ of\ control}\right) \times 100 \tag{2}$$

$$\text{Viability}\% = 100 - \text{Toxicity}\% \tag{3}$$

2.5. Molecular docking studies

To model the target proteins, we utilized the amino acid sequences obtained from the UniProt database (TNF: P01375 and MMP9: P14780 (organism: Human), EBNA1: P03211 and LMP1: P03230 (organism: Epstein-Barr virus)) and employed the SWISS-MODEL automatic homology modeling servers [36–40]. The generated models were subsequently refined using the SPDBV software, employing energy minimization techniques [41–44]. This process allowed for the improvement and optimization of the protein models for further analysis and study. To perform docking between the macromolecule and ligands, we utilized AutoDock 4.0 (1.5.6) (The Scripps Research Institute, La Jolla, CA, USA), which applies relevant algorithms to the system. The docking process was executed

multiple times (100 times) for each ligand, using the Cygwin 64 Terminal. This allowed for a comprehensive exploration of the binding interactions between the ligands and the target protein, providing valuable insights into their potential inhibitory effects.

2.6. Molecular dynamic

The simulation for best ligands with less energy in molecular docking study was carried out using GROMACS 2021 with Ubuntu 24.04 Linux, running on an Intel core 14, and with 32 GB RAM for 200 ns. The topology and coordinate files were generated using the Charmm36 force field by gmx pdb2gmx and the SwissParam server for the protein and ligands, respectively. In detail, each system was placed in a cubic box filled with (TIP3P) water molecules under periodic boundary conditions, with a 1 nm distance from each edge. In the subsequent stage, energy minimization was carried out in 50,000 steps for 2 fs. Then, the system was equilibrated at a stable temperature of 310 K using the Berendsen temperature algorithm and pressure of 1 bar in the NVT NPT ensembles. Root-mean-square deviation (RMSD), root mean square fluctuation (RMSF), radius of gyration (RG), solvent accessible surface area (SASA), hydrogen bond analysis, Molecular mechanics Poisson–Boltzmann surface area (MM-PBSA) were calculated to analyze the trajectories. All parameters and analysis presented in the results are the average values of replicates.

3. Results

3.1. Synthesis of gold nanoparticles

In the majority of cases involving gold nanoparticle synthesis from plant extract, the resulting solution adopts a characteristic purple color, signifying the successful formation of nanoparticles due to the unique optical properties of gold.The UV spectrum of the samples within the 500–600 nm range reveals a distinct peak, specifically around 540 nm, providing compelling evidence of successful gold nanoparticle synthesis, as depicted in Fig. 1.

To investigate the presence and binding of biomolecules to the synthesized gold nanoparticles, confirming the role of plant extract in reducing gold ions and stabilizing the nanoparticles, IR spectra of the synthesized gold nanoparticle solution and the extract powder were examined (see Fig. 2). To investigate the presence and attachment of biomolecules to synthesized gold nanoparticles and confirm the role of plant extract in reducing gold ions and the formation and stability of gold nanoparticles, the IR spectra of the dissolved powder of the synthesized gold nanoparticles and the dissolved powder of the extract were analyzed. The analysis of the IR spectra revealed several important findings.

Firstly, the presence of wide and intense absorption peaks in the range of 3834.40 and 3423.86 cm^{-1} indicated the presence of stretching vibrations in the alcohol functional group. This suggests the presence of alcohols or compounds containing hydroxyl groups in both the synthesized nanoparticles and the plant extract. Furthermore, the presence of bands at 1612.67 and 1638.46 cm^{-1} in both spectra indicated the presence of carbon-carbon unsaturated double bonds. These bonds are characteristic of functional groups such as carbonyl, alkene, aldehyde, and ester. This finding suggests the presence of these functional groups in both the synthesized nanoparticles and the plant extract.

Moreover, the spectrum of the plant extract exhibited peaks at 1064.15 cm^{-1} and 1377.57 cm^{-1}, indicating the presence of stretching and bending vibrations of functional groups such as anhydride, carboxylic acid, and alcohol. However, these peaks were either absent or weakened in the spectrum of the synthesized nanoparticles. This suggests that the bonds between gold ions and the plant compounds, including carbonyl biomolecules, flavonoids, tannins, and other phenolic compounds present in the plant extract, have been formed during the reduction of gold ions and the formation of gold nanoparticles. These findings provide evidence for the involvement of specific biomolecules in the reduction of gold ions and the stabilization of gold nanoparticles. The plant extract appears to play a significant role in this process by providing functional groups that can interact with gold ions and facilitate their reduction

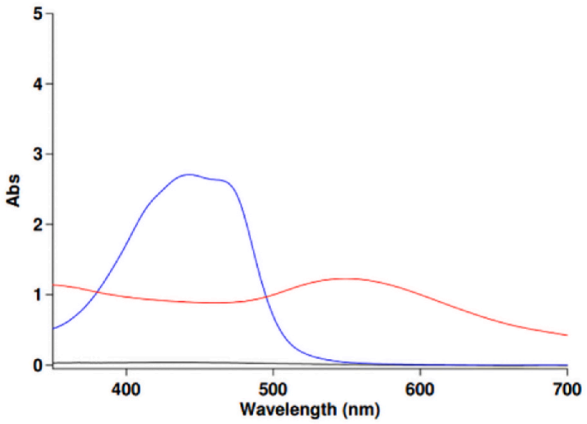

Fig. 1. UV–VIS spectrums of black) purified water, blue) saffron extract, and red) saffron nanoparticle.

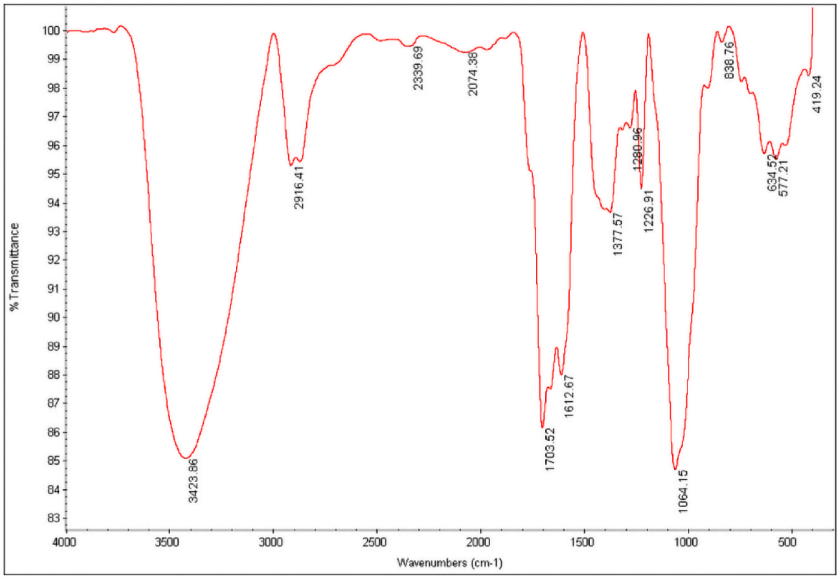

Fig. 2. FT-IR (T) spectrum of saffron extract.

and subsequent nanoparticle formation. Overall, the IR spectra analysis supports the hypothesis that the plant extract acts as a reducing agent and stabilizer in the synthesis of gold nanoparticles. The presence of alcohol functional groups and carbon-carbon unsaturated double bonds in both the nanoparticles and the plant extract suggests their involvement in the reduction and stabilization processes (see Fig. 3).

XRD results for gold nanoparticles exhibit four peaks at approximately 39, 44 and 65°, and 78°, aligning with standard gold peaks and thereby validating the accuracy of gold nanoparticle synthesis that is shown in Fig. 4. The size of the synthesized nanoparticles, determined through transmission electron microscopy (TEM), is less than 5 nm, featuring both spherical and polyhedral shapes is shown in Fig. 5

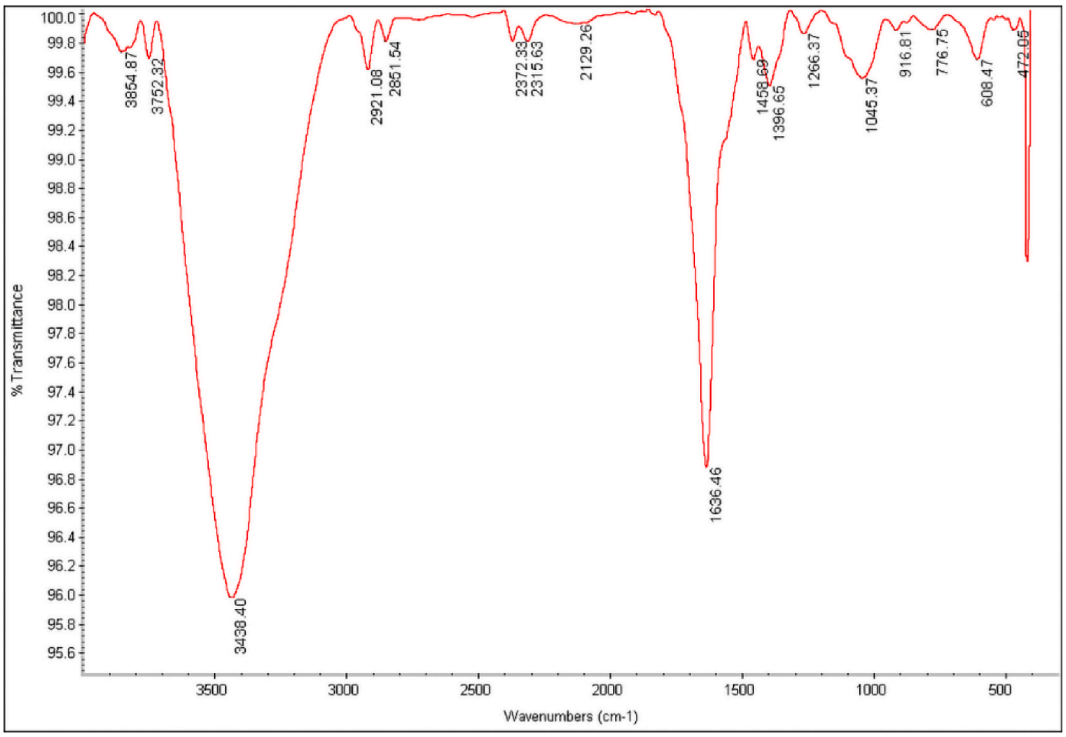

Fig. 3. FT-IR (T) spectrum of saffron nanoparticle.

The zeta potential is a measure of the stability of colloidal dispersions (see Fig. 6). The measured potential for the freshly prepared solution was equal to −16.3 mV. A negative zeta potential indicates that the nanoparticles have a net negative charge. Values between −10 and −30 mV imply moderate stability. thus, value of −16.3 mV suggests that the nanoparticles are somewhat stable. Also, electrophoretic mobility for this solution was −0.000126 cm^2/Vs. Electrophoretic mobility is related to how fast the particles move in an electric field, with the negative value indicating movement towards the positive electrode. This value, being quite small, aligns with the mild mobility of the nanoparticles which is consistent with the moderate zeta potential. It can also give an indication of the zeta potential; this small number indicates that although there is a charge on the nanoparticles, the resulting mobility is limited, which can be due to particle size or viscosity of the medium.

Dynamic Light Scattering (DLS) result for fresh solution is 269.6 nm and Polydispersity Index (PI) was 0.630, which reflects the hydrodynamic diameter of the nanoparticles, including any surface adsorbed layer of solvent. This suggests that the nanoparticles are relatively large and could potentially form aggregates, which is supported by the zeta potential results. The polydispersity index indicates the size distribution of the particles in the sample. A PI value below 0.1 is considered monodispersed and implies a tight size distribution; the value of 0.630 reveals a polydispersed dispersion, meaning there are significant variations in particle size. This could contribute to the stability issues reflected in the zeta potential. These cases can be justified by the acidic pH of saffron, because at acidic pH, gold nanoparticles aggregate.

Zeta potential for one year solution was −13.3 mV and electrophoretic mobility was −0.000104 cm^2/Vs, the zeta potential has increased towards zero, indicating a decrease in the negative charge. This reduction can suggest that the nanoparticles are losing their charge stability over time, which may lead to increased potential for aggregation. The mobility has decreased, which is consistent with the decrease in zeta potential. This reduction indicates a lower rate of movement under an electric field, corresponding to the observed minor loss in charge stability.

Also, DLS for One Year Solution and its PI were 327 nm and 0.601, the average size of the nanoparticles has increased, indicating possible aggregation or growth of particles over the year. the PI has decreased slightly, suggesting a slight improvement in the uniformity of the size distribution of particles. However, the overall increase in size and the PI being above 0.5 indicates that the sample still exhibits a significant degree of polydispersity.

The capacity of the rose water extract, plant-extract-based synthesized gold nanoparticles, and ascorbic acid as a standard to absorb free radicals (DPPH) was examined in 517 nm and reported in Table 1. Additionally, the absorption graph against concentration was plotted. As concentration increased, the absorption level decreased, visually observed by the diminishing purple color resulting from the DPPH solution. This indicated the neutralization of DPPH by the antioxidant compounds present in the solutions (see Table 2).

Subsequently, the radical scavenging capacity (RSC%) for each sample solution was calculated using the following formula, and the graph was plotted to determine the RSC50 %, representing the concentration at which the solution neutralizes at least 50 % of free radicals.

$$\mathrm{RSC\%} = \frac{(A_0 - A_x)}{A_0} \times 100 \tag{4}$$

Where (A_0) is Absorption of DPPH solution and (A_x) is Absorption of sample solutions. The graph revealed the RSC50 % concentration for ascorbic acid as 22.72 ppm, for gold nanoparticles as 92.40 ppm, and the plant extract as 105.60 ppm. Consequently, the antioxidant potency of saffron water compounds increased following binding with gold nanoparticles.

3.2. Antibacterial properties

After synthesizing gold nanoparticles using plant extract, we observed significant improvements in antibacterial properties. The initial antibacterial activity percentage against Gram-negative bacteria (E. Coli) with the plant extract was 52.37 % which increased notably to 89.67 % after nanoparticle synthesis. Likewise, the antibacterial activity percentage for Gram-positive (S. Aureus) bacteria

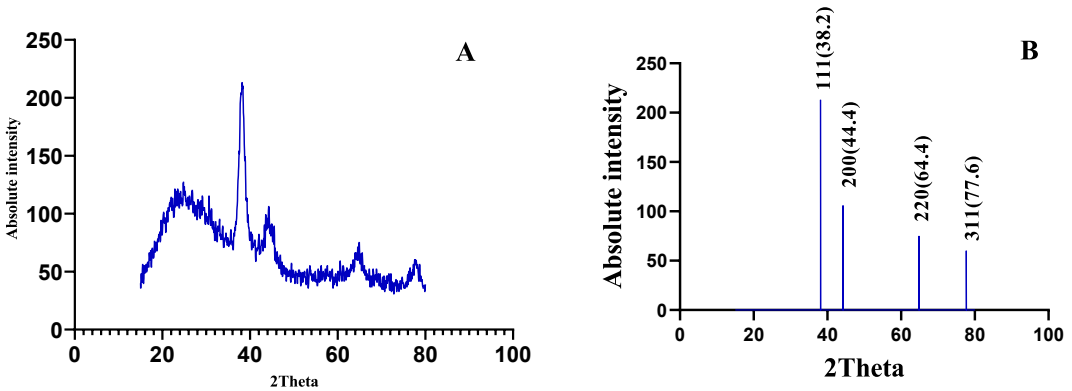

Fig. 4. XRD spectrum of **A)** saffron nanoparticle and **B)** The XRD patterns of AuNP.

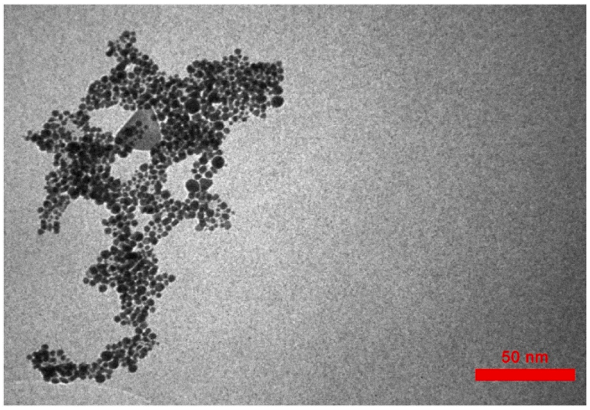

Fig. 5. TEM pictures of saffron nanoparticles.

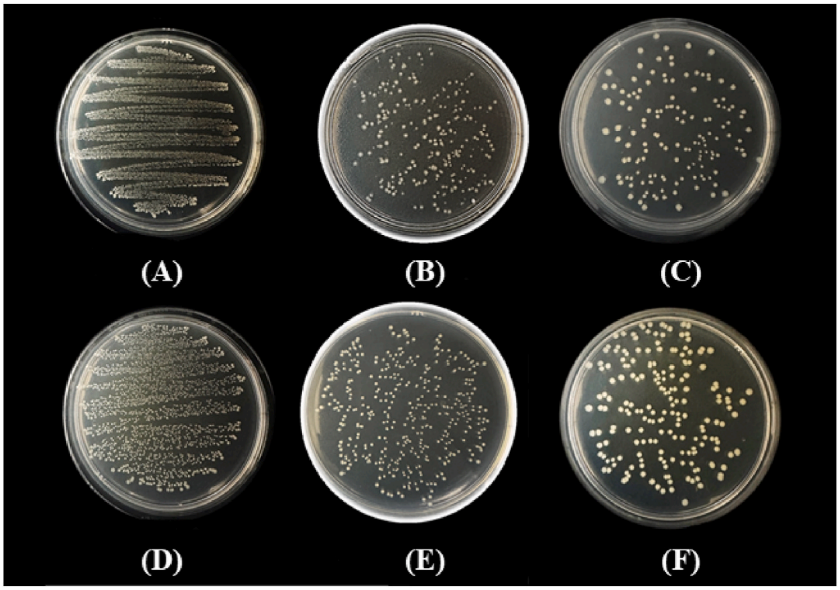

Fig. 6. Antibacterial tests: **(A),** E. Coli control **(B),** E. Coli exposed to saffron extract **(C),** E. Coli exposed to saffron nanoparticle **(D)** S. Aureus control **(E),** S. Aureus exposed to saffron extract **(F),** S. Aureus exposed to saffron nanoparticles.

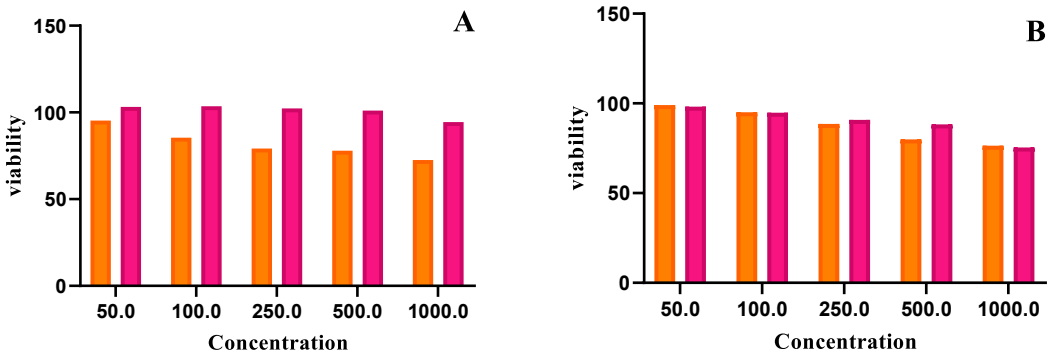

Fig. 7. A, Viability chart by concentration (μg/mL) of extract (orange) and nanoparticle (pink) for C6 cells and **B,** SH-SY5Y cells.

Table 1
Absorption of each sample in 517 nm.

C (ppm)	Ascorbic acid	Extract	Nanoparticle
31.25	0.6364	0.7658	0.7572
62.5	0.5132	0.6661	0.6342
125	0.393	0.5364	0.521
250	0.2116	0.4066	0.3735
DPPH Concentration: 40 ppm		DPPH Absorbance: 1.2242	

Table 2
The radical scavenging capacity for each sample solution.

C (ppm)	Ascorbic acid	Extract	Nanoparticle
31.25	48.02 %	37.44 %	38.15 %
62.5	58.08 %	45.59 %	48.19 %
125	67.90 %	56.18 %	57.44 %
250	82.72 %	66.79 %	69.49 %

increased from 43.93 % with the plant extract to approximately double, reaching 83.26 % following the synthesis process.

3.3. MTT

The cytotoxicity findings on the C6 cell line highlight the ability of plant-based nanoparticle synthesis to a notable and substantial reduce the toxicity of these compounds. The cytotoxicity test results on the SH-SY5Y cell line emphasize a reduction in the toxicity of saffron extract compounds through nano-sizing at elevated concentrations. Remarkably, this has led to a significant increase in cell growth in certain instances compared to the control cells (see Table 3).

3.4. Molecular docking studies

Based on the findings that are reported in Table 4, the compounds chlorogenic acid, gallic acid, HTCC, linolenic acid, and safranal exhibit the best binding energies of −8.44, −8.3, −7.14, −6.96, and −6.79, respectively, in inhibiting the TNF. Among the compounds evaluated, quercetin, chlorogenic acid, linolenic acid, kaempferol, and safranal exhibit the best binding energies of −8.98, −8.23, −7.96, −7.22, and −6.61, respectively for MMP9. According to ccT, chlorogenic acid, EGCG, isoquercetin, quercetin, and picrocrocin demonstrate the best binding energies for EBNA1, with values of −10.72, −10.02, −9.56, −7.66, and −7.31 respectively and isoquercetin, EGCG, chlorogenic acid, picrocrocin, and quercetin exhibit the best binding energies for LMP1, with values of −9.11, −8.7, −7.99, −7.81 and −7.12, respectively.

The cells marked with asterisks (*) in the table refer to the compound crocin. However, due to its large size and significant weight, it may not be feasible to investigate this particular compound using computational tools such as Auto Dock. Additionally, its high weight may prevent it from meeting Lipinski's rule, which could indicate limitations in studying its inhibitory effects. It may be necessary to explore alternative experimental approaches to further investigate the potential of crocin as an inhibitor.

Table 5 analyzes the chemical and biochemical properties of the compounds of interest, taking into consideration several important factors. The SwissADME database primarily focuses on lipophilicity, size, compound flexibility, and solubility. Lipophilicity is the ability of a chemical compound to dissolve in fats, oils, lipids, and non-polar solvents. A value closer to 5 suggests that the compound is more likely to effectively cross cell membranes. This property is significant as it impacts the compound's ability to interact with target proteins and exert its desired effects. The water solubility of the compound is also predicted to assess the feasibility of investigating water-soluble drug formulations, if applicable. Water solubility is crucial for drug delivery systems and ensuring the compound's effective dissolution in the body. The size of the compounds, represented by their molecular weight, is another important consideration. To be considered suitable as a drug compound, the molecular weight should typically be less than 500 g per mole. This criterion ensures that the compound is small enough for efficient absorption, distribution, metabolism, and excretion within the body. Furthermore, the flexibility of the compounds is assessed by evaluating the number of rotatable bonds they possess. Flexibility impacts

Table 3
IC50 parameters.

Parameters	C6 Cells		SH-SY5Y Cells	
	Extract	Nanoparticle	Extract	Nanoparticle
IC50	7505	1207	4267	3703
Degrees of freedom	3	3	3	3
R Squared	0.8743	0.479	0.9435	0.9653
Sum of squares	37.72	29.24	20.87	10.62

Table 4
Gibbs free energy values obtained from the docking of each compound with the proteins (kcal/mol).

C.No	Compound Name	MMP-9	TNF	LMP1	EBNA1
1	Chlorogenic acid	−8.23	−8.44	−7.99	−10.72
2	Crocetin	4.33	95.14	−4.8	−6.81
3	Crocin	*	*	*	*
4	Epigallocatechin Gallate	−4.77	9.71	−8.7	−10.02
5	Gallic acid	−5.95	−8.3	−4.6	−6.64
6	HTCC	−5.44	−7.14	−4.66	−4.9
7	Isoquercetin	−5.29	1.86	−9.11	−9.56
8	Kaempferol	−7.22	−6.36	−6.35	−6.46
9	Linolenic acid	−7.96	−6.96	−4.46	−6.15
10	Picrocrocin	−6.61	0.94	−7.81	−7.31
11	Quercetin	−8.98	−5.3	−7.12	−7.66
12	Safranal	−6.48	−6.79	−4.6	−5.15

Table 5
The results of the pharmacokinetic studies of the compounds based on the SwissADME.

C. No	Mw (g/mol)	H-bond donors	H-bond acceptor	MLOGP	LIPO	Fraction Csp3	rotatable bonds	TPSA (Å)	Water Solubility	GI.Abs	BBB Permineat	P-gp substrate	CYP inhibitors	Lipinski	Bio.score
1	354.31	6	9	-1.05	-0.39	0.04	5	164.75	Soluble	Low	No	No	No	NH OR OH	0.11
2	328.4	2	4	-1.05	-0.39	0.2	8	74.60	Soluble	Low	No	No	No	NH OR OH	0.11
3	977	*	*	*	*	*	*	*	*	*	*	*	*	*	*
4	458.37	8	11	-0.44	0.95	0.14	4	197.37	Soluble	Low	No	No	No	NH OR OH	0.17
5	170.12	4	5	7.84	0.21	0.00	1	97.99	Soluble	High	No	No	3A4	Yes	0.56
6	168.23	1	2	1.27	1.6	0.7	1	37.30	very soluble	High	Yes	No	No	Yes	0.55
7	464.38	8	12	-2.59	-0.48	0.29	4	210.51	Soluble	Low	No	No	No	NH OR OH	0.17
8	286.24	4	6	-0.03	1.58	0.00	1	111.13	Soluble	High	No	Yes	1A2 2D6 3A4	Yes	0.55
9	278.43	1	2	-0.03	1.58	0.61	13	37.30	Soluble	High	No	Yes	1A2 2D6 3A4	Yes	0.55
10	330.37	4	7	-0.88	0.02	0.81	4	116.45	Very soluble	High	No	Yes	No	Yes	0.55
11	302.24	5	7	-0.56	1.23	0.00	1	131.36	Soluble	High	No	No	1A2 2D6 3A4	Yes	0.55
12	150.22	0	1	2.10	2.3	0.5	1	17.07	Soluble	High	Yes	No	No	Yes	0.55

the compound's conformational changes and its ability to interact with target proteins accurately. These factors provide valuable insights into the chemical and biochemical properties of the compounds, enabling researchers to evaluate their potential as drug candidates and guide further investigations (see Fig. 8).

Based on the findings that are reported in Table 5, among these compounds, HTCC and safranal are anti-inflammatory compounds capable of crossing the blood-brain barrier, indicating their potential effectiveness in inhibiting TNF. However, it is important to note

that chlorogenic acid violates Lipinski's 5th rule in terms of the number of donor hydrogen bonds. Furthermore, linolenic acid's interaction with metabolic enzymes CYP1A2, CYP2D6, and CYP3A4 may render it unsuitable as a potential drug candidate for inhibiting this protein.Considering these factors, gallic acid, HTCC, and safranal emerge as the most favorable compounds for inhibiting the TNF while also complying with Lipinski's 5th rule. In Fig. 9-a, it is evident that gallic acid forms six hydrogen bonds with the tumor necrosis factor protein. Three of these hydrogen bonds are established with the B chain, specifically with tyrosine 195 (bond lengths of 2.195 and 2.301 Å) and proline 193 (bond length of 1.883 Å). Gallic acid also forms two hydrogen bonds with lysine 174 of chain C (bond lengths of 2.036 and 2.385 Å) and one with lysine 174 of chain A (bond length of 1.686 Å), resulting in a favorable binding energy. In Fig. 9-b, it is observed that HTCC establishes two hydrogen bonds with lysine 174 of chain C (bond length of 2.016 Å) and tyrosine 195 of chain B (bond length of 1.918 Å). Lastly, according to Fig. 9-c, safranal forms a single hydrogen bond with tyrosine 195 of chain C (bond length of 1.878 Å) (see Fig. 10).

Pharmacokinetic studies suggest that while chlorogenic acid forms a strong connection with MMP9 in terms of the number of donor hydrogen bonds, it violates Lipinski's 5th rule. This violation raises concerns about its suitability as a potential drug compound. On the other hand, safranal demonstrates anti-inflammatory properties and the ability to cross the blood-brain barrier, indicating its potential for a good inhibitory effect on the targeted inflammatory protein. Quercetin and safranal emerge as the most suitable compounds for inhibiting the protein, as they meet all the criteria outlined by Lipinski's 5th rule. Although linolenic acid and kaempferol inhibit metabolic enzymes CYP1A2, CYP2D6, and CYP3A4, they may not be considered appropriate compounds. However, considering its better binding energy, linolenic acid can be selected as the third compound in this context. These findings suggest that quercetin, safranal, and linolenic acid hold promise as potential inhibitors of the target protein based on their favorable binding energies and adherence to Lipinski's rule, while caution should be exercised in considering chlorogenic acid and kaempferol as potential drug candidates for inhibiting this protein. In Fig. 9-d, it is observed that the arginine 51 and 36 contribute a total of 4 hydrogens in the bond formation, resulting in the establishment of 4 hydrogen bonds with quercetin. This indicates a strong interaction between quercetin and the protein. In Fig. 9-e, linolenic acid forms a hydrogen bond with proline 415, with a bond length of 2.173 Å. Additionally, it forms two hydrogen bonds with arginine 424. These interactions further contribute to the favorable binding energy between Linolenic acid and the protein. As observed in Fig. 9-f, it appears that safranal does not form any hydrogen bonds with the MMP9 protein. The lack of hydrogen bonding interactions between safranal and the protein may suggest a weaker binding affinity compared to compounds that do form hydrogen bonds.

However, it is important to note that chlorogenic acid, EGCG, and isoquercetin violate Lipinski's 5th rule, which raises concerns about their suitability as potential drug candidates for targeting EBNA1. Therefore, quercetin and picrocrocin are considered the most suitable compounds for inhibiting EBNA1, as they comply with Lipinski's 5th rule. In Fig. 9-g, it is observed that quercetin forms two hydrogen bonds with arginine 521, with bond lengths of 1.951 and 2.638 Å. Additionally, it forms another hydrogen bond with asparagine 475, with a bond length of 2.251 Å. These interactions demonstrate the potential of quercetin to inhibit the protein and hinder the growth and proliferation of the Epstein-Barr virus, which is responsible for inflammation and latent infection. Similarly, picrocrocin, as depicted in Fig. 9-h, forms two hydrogen bonds with asparagine 475. It also forms bonds with glycine 473, arginine 521, and glycine 470, with bond lengths of 2.283, 2.133, 1.906, 2.172 and 2.043 Å, respectively. These interactions further contribute to the potential inhibitory effect of picrocrocin on EBNA1.

However, it is important to note that chlorogenic acid, EGCG, and isoquercetin violate Lipinski's 5th rule, which raises concerns about their suitability as potential drug candidates for targeting LMP1. Therefore, quercetin and picrocrocin are considered the most favorable compounds for inhibiting LMP1, as they comply with Lipinski's 5th rule. Based on Fig. 9-i, it can be observed that quercetin forms two hydrogen bonds with tyrosine 186 and glutamine 205, with bond lengths of 1.932 and 2.159 Å, respectively. These hydrogen bonds indicate a strong interaction between quercetin and the protein, suggesting its potential effectiveness in targeting LMP1. Additionally, as depicted in Fig. 9-j, picrocrocin forms two hydrogen bonds with glutamine 206 and tyrosine 186, with bond lengths of 1.876, 1.992, and 1.919 Å, respectively. These hydrogen bonds further support the potential of picrocrocin as a candidate for targeting LMP1. Both quercetin and picrocrocin show promise as potential compounds for inhibiting LMP1, and their compliance with Lipinski's 5th rule adds to their favorable characteristics.

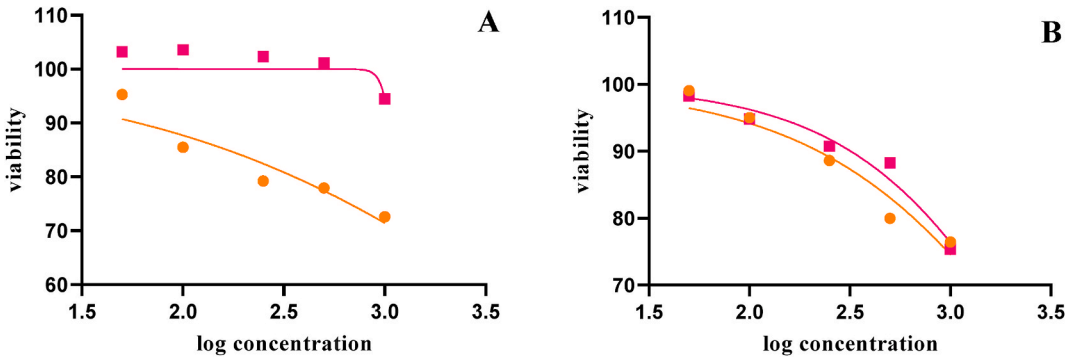

Fig. 8. **A,** Viability chart by log concentration of extract (orange) and nanoparticle (pink) for C6 cells and **B,** SH-SY5Y cells.

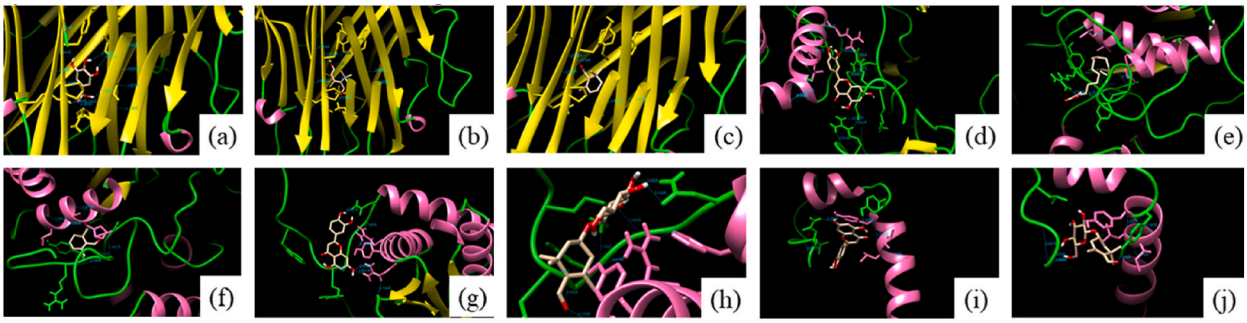

Fig. 9. a, gallic acid docked with TNF **b,** HTCC docked with TNF **c,** safranal docked with TNF **d,** quercetin docked with MMP9 **e,** linolenic acid docked with MMP9 **f,** safranal docked with MMP9 **g,** quercetin docked with EBNA1 **h,** picrocrocin docked with EBNA1 **i,** quercetin docked with LMP1 **j,** picrocrocin docked with LMP1.

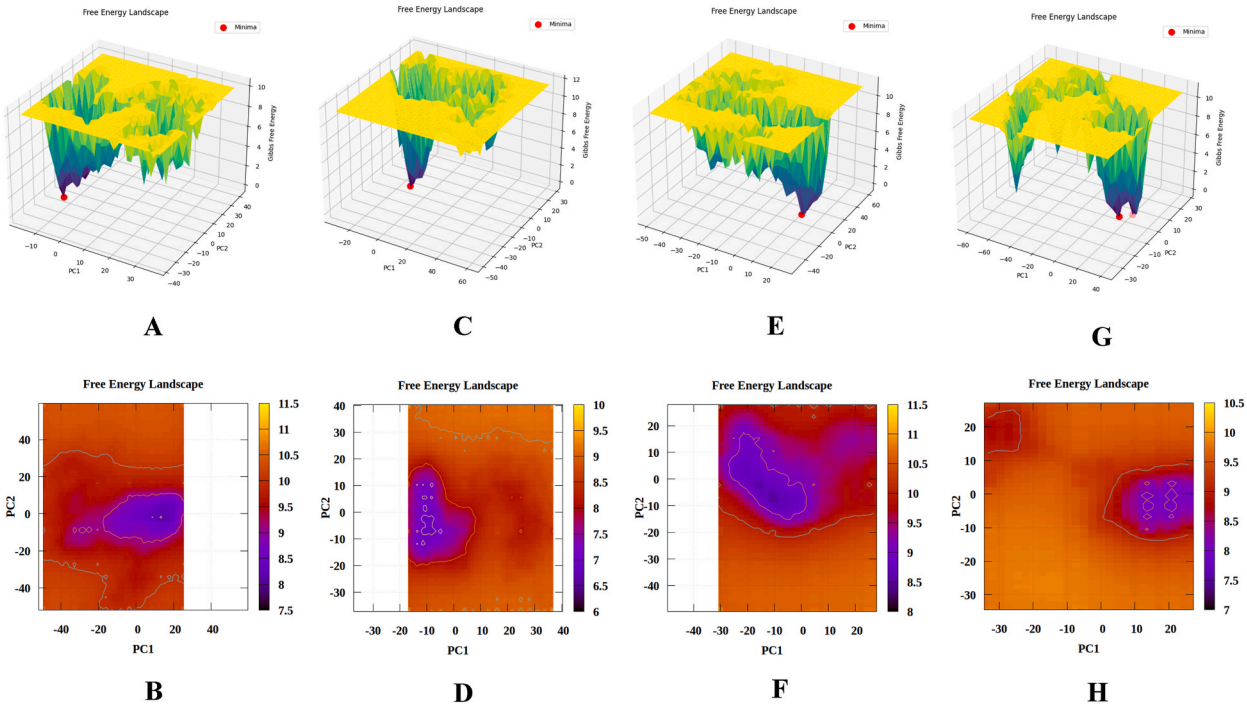

Fig. 10. Free energy landscape with minima for **A, B)** MMP9 **C, D)** Chlorogenic acid **E, F)** Linolenic acid and **G, H)** Quercetin.

3.5. Molecular dynamic

Molecular dynamics (MD) simulations offer a powerful approach to studying the temporal behavior of molecules. Key parameters, including Root Mean Square Deviation (RMSD), Root Mean Square Fluctuation (RMSF), Radius of Gyration (RG), and Solvent Accessible Surface Area (SASA), are instrumental in analyzing the structural and dynamic properties of molecular systems. RMSD quantifies the average displacement of atoms (commonly the backbone atoms of a protein) from a reference structure over time. It is widely used to evaluate the stability of a protein during simulations, indicating the extent of deviation from its initial conformation. RMSF measures the average deviation of individual atoms from their mean positions during the simulation. This parameter provides insights into the flexibility of specific residues or atoms, highlighting regions of increased mobility or structural stability. RG describes the compactness of a molecular structure by measuring how closely atoms are clustered around their center of mass. Changes in RG can reveal conformational shifts and alterations in structural integrity throughout the simulation. SASA quantifies the surface area of a molecule that is exposed to solvent. Variations in SASA during MD simulations can reflect the exposure of hydrophobic residues or the occurrence of ligand-binding events, making it a critical metric for studying protein-protein and protein-ligand interactions. MD simulations are particularly useful in identifying active sites in proteins through several analytical approaches. Regions with high RMSF values may correspond to flexible or allosteric sites. Clustering MD trajectories can reveal conformational states that expose or conceal potential active sites. Additionally, visualization tools can track changes in the geometry and solvent exposure of active sites

over time. Monitoring hydrogen bond interactions during simulations further elucidates how ligand interactions evolve within active sites. These molecular dynamics parameters are essential for interpreting the outcomes of MD simulations. They provide valuable insights into protein dynamics, flexibility, and interactions, thereby facilitating the identification of potential active sites and advancing our understanding of molecular mechanisms (see Figs 16–20)

RMSD (Fig. 11) measures of the MMP-9 with chlorogenic acid show moderate stability, but still fluctuate over time and linolenic acid demonstrates better stabilization of the protein-ligand complex compared to chlorogenic acid. Quercetin displays the lowest RMSD values, indicating the most stable complex. RMSF evaluates fluctuations in specific residues. Quercetin reduces residue flexibility, especially in the active site region, making it a strong inhibitor. While, chlorogenic acid has moderate residue fluctuations and Linolenic Acid Shows less residue stability than quercetin. Also, quercetin forms the highest number of hydrogen bonds with MMP9 over time, which contributes to its inhibitory effect and structural stability but linolenic acid and Chlorogenic Acid form fewer hydrogen bonds. Radius of Gyration (RG) indicates the compactness of the protein-ligand complex, quercetin results in the most compact structure. Linolenic acid and chlorogenic acid are less compact than quercetin. Also, quercetin reduces the SASA value significantly, which indicates less exposure of hydrophobic regions to the solvent and stronger binding. Zinc Ion which is the central component of the active site and essential for the catalytic activity of MMP9. It coordinates with specific residues (e.g., His401, His405, and Glu402) to form the catalytic machinery. Catalytic water molecule which positioned close to the zinc ion, plays a key role in hydrolysis reactions. In addition, S1′ Pocket, a hydrophobic pocket near the zinc-binding site, substrates and inhibitors typically interacts with this pocket, which determines the specificity of the enzyme. The flexibility of residues around the active site (e.g., loop regions) affects substrate binding and inhibitor efficacy. Quercetin strongly stabilizes the active site, forms hydrogen bonds with key residues like Glu402 or water molecules near the zinc ion, and reduces flexibility of the catalytic residues, preventing substrate access. May partially block the S1′ pocket, making it highly effective as an inhibitor. Chlorogenic acid, forms moderate hydrogen bonds with residues near the active site and has weaker interactions with the zinc ion compared to quercetin, which may reduce its effectiveness. Stabilizes the active site but allows more flexibility compared to quercetin. Linolenic acid, interacts primarily through hydrophobic contacts, rather than specific hydrogen bonding and does not strongly interact with the zinc ion or catalytic residues, limiting its ability to inhibit MMP9 effectively. May reduce overall flexibility of the active site but does not block it as effectively as quercetin (see Fig. 13) (see Fig. 12).

Among the analyzed ligands, HTCC demonstrated the most stable binding, as evidenced by its minimal fluctuations over the simulation timeframe. Also, HTCC showed the lowest Rg (Fig. 14) values, indicating a compact protein-ligand complex structure. This implies that HTCC induces minimal conformational changes in TNF, likely maintaining the protein's integrity while interacting with its active site. The number of hydrogen bonds formed between HTCC and the TNF protein was consistently higher compared to other ligands, such as gallic acid and chlorogenic acid. This robust H-bond network contributes to HTCC's superior binding affinity. HTCC's interaction appeared to stabilize the active site residues, potentially blocking the site more effectively than other ligands. This suggests HTCC as the most potent inhibitor in this study. HTCC exhibited strong and stable interactions with the key residues of the active site. It formed multiple hydrogen bonds and hydrophobic interactions, which stabilized the conformation of the active site. RMSF analysis revealed minimal fluctuations in the active site residues in the presence of HTCC. This indicates that HTCC effectively restricted the mobility of the active site, making it the most potent inhibitor among the studied ligands (see Fig. 15).

EGCG forms multiple hydrogen bonds with critical residues in the primary binding pocket, stabilizing the active site in an inactive conformation. Chlorogenic acid interacts through fewer hydrogen bonds and hydrophobic contacts with active site residues and isoquercetin forms intermediate interactions with the primary and secondary binding pockets. The active site of LMP1 is most effectively targeted by EGCG, which stabilizes the key residues, displaces catalytic water molecules, and blocks substrate binding through strong interactions. Chlorogenic acid and isoquercetin also interact with the active site but are less effective in inducing structural changes necessary for inhibition (see Fig. 19).

RMSF (Fig. 20) data suggests that residues in the active site are most stabilized by EGCG, indicating reduced flexibility, which is critical for effective inhibition. Chlorogenic acid showed moderate stabilization, while isoquercetin exhibited the least impact, with higher residue flexibility observed. EGCG forms stable hydrogen bonds and hydrophobic interactions with critical residues, such as Tyr, Arg, and Asp, which are involved in maintaining the active site's structure and functionality. Chlorogenic acid interacted with a subset of these residues but with less strength, while isoquercetin displayed weaker interactions overall. EGCG despite computational challenges in energy normalization, EGCG demonstrated strong interactions in MD simulations, which suggest its high binding affinity. Chlorogenic acid displayed moderate binding energies and interactions and isoquercetin showed the least favorable binding energies, indicating weaker inhibition. EGCG induces a more compact protein structure, as indicated by a smaller RG value, which suggests that the protein assumes a more folded and rigid conformation upon binding. This compactness is indicative of a more stable and

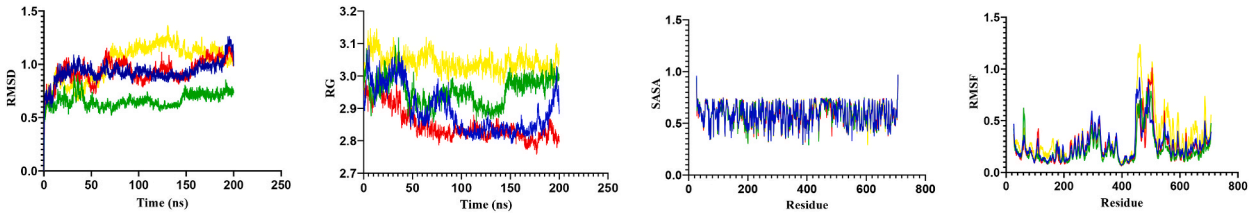

Fig. 11. MD analysis of **(blue)** MMP9, **(green)** Chlorogenic acid, **(red)** Linolenic acid, and **(yellow)** Quercetin. RMSD, RG, SASA and RMSF.

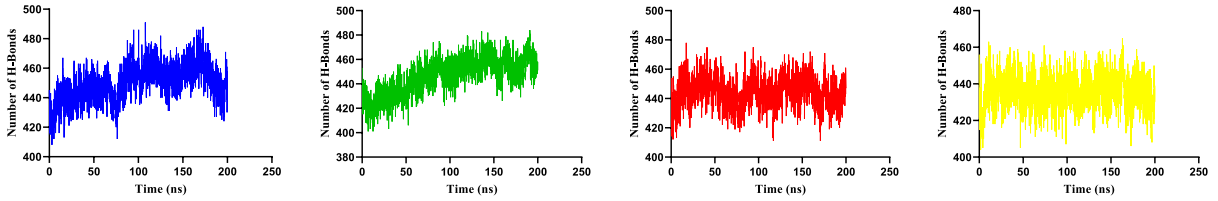

Fig. 12. H-Bond of **(blue)** MMP9, **(green)** Chlorogenic acid, **(red)** Linolenic acid, and **(yellow)** Quercetin.

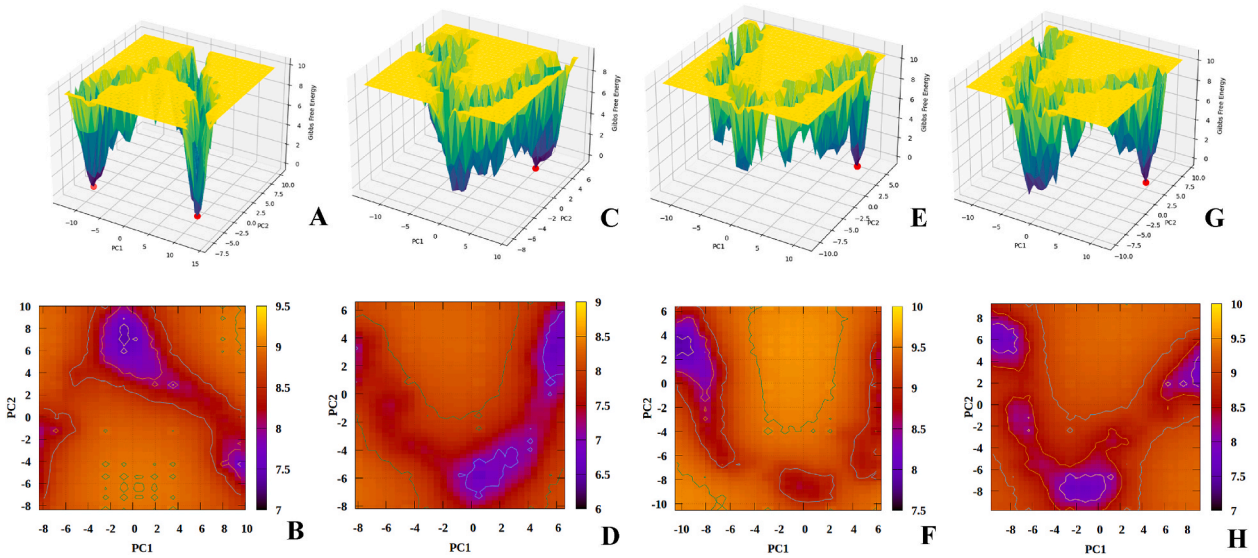

Fig. 13. Free energy landscape with minima for **A, B)** TNF **C, D)** Chlorogenic acid **E, F)** HTCC and **G, H)** Gallic acid.

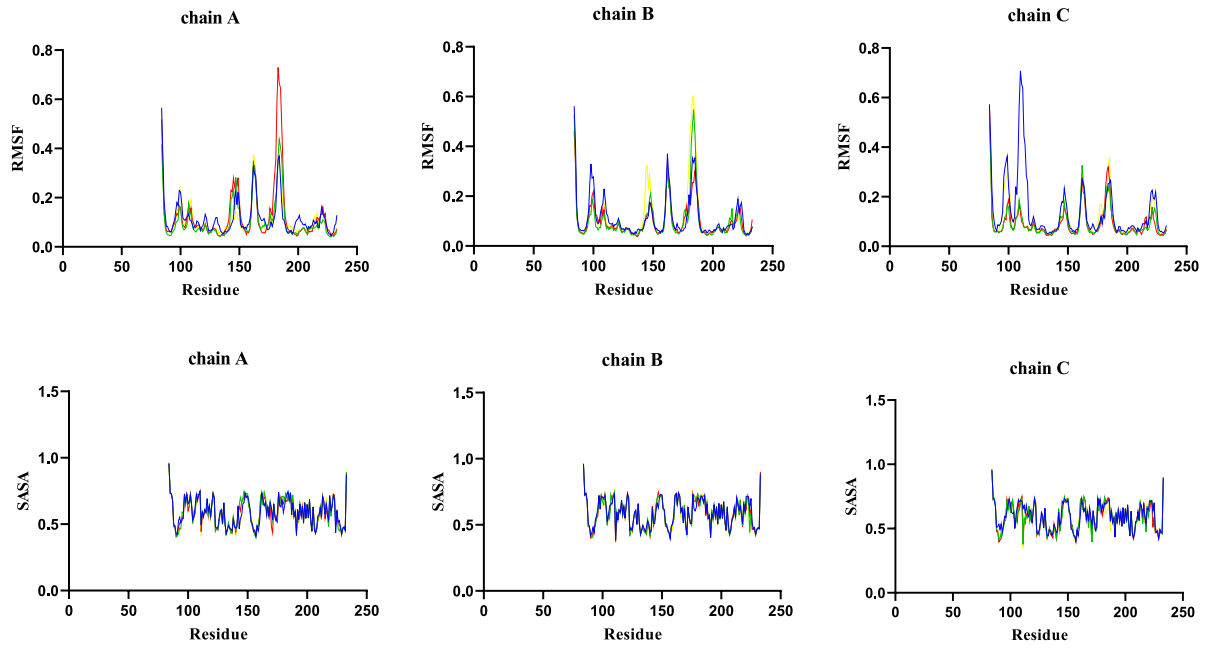

Fig. 14. MD analysis of **(blue)** TNF, **(green)** Chlorogenic acid, **(red)** HTCC, and **(yellow)** Gallic acid.

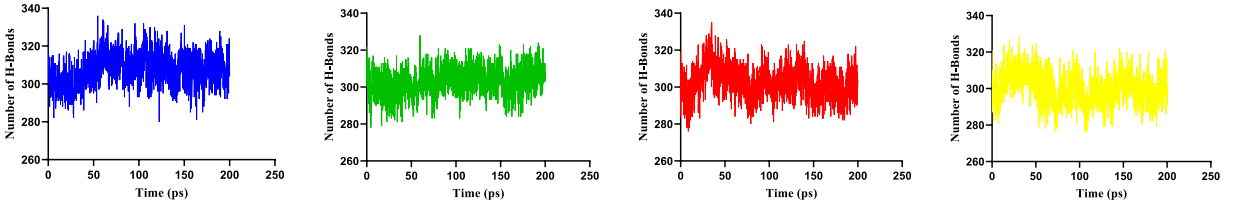

Fig. 15. H-Bond of **(blue)** TNF, **(green)** Chlorogenic acid, **(red)** HTCC, and **(yellow)** Gallic acid.

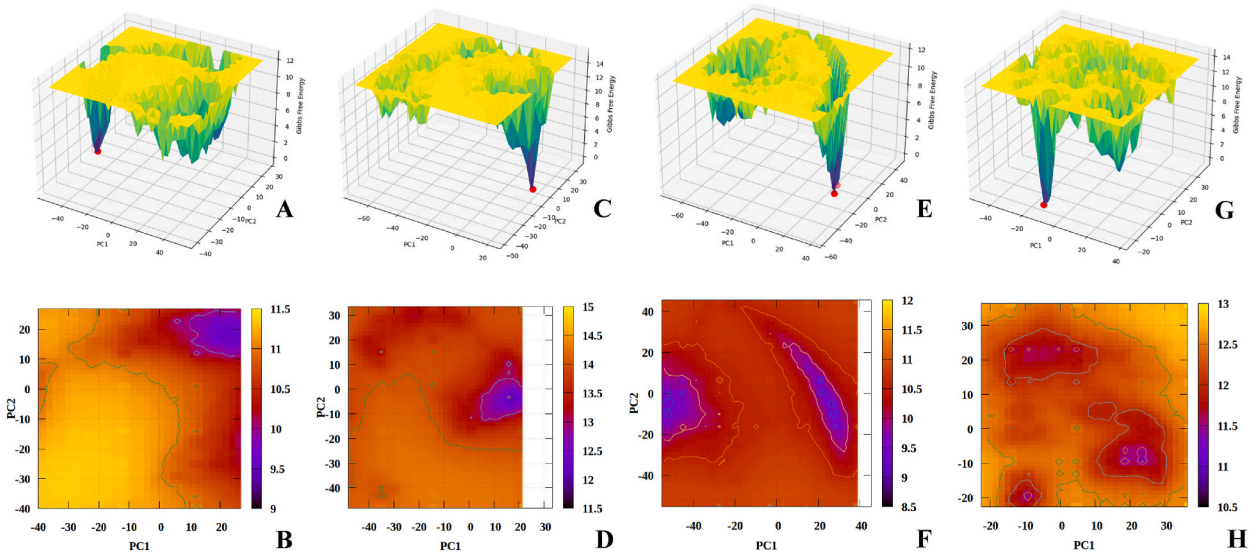

Fig. 16. Free energy landscape with minima for **A, B)** LMP-1 **C, D)** Chlorogenic acid **E, F)** EGCG and **G, H)** Isoquercetin.

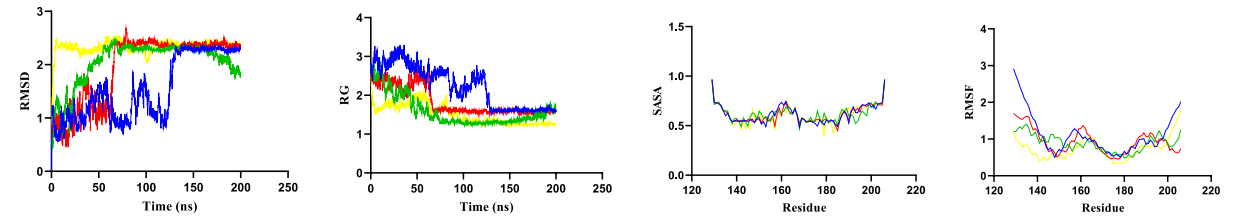

Fig. 17. MD analysis of **(blue)** LMP-1, **(green)** Chlorogenic acid, **(red)** EGCG, and **(yellow)** Isoquercetin. RMSD, RG, SASA and RMSF.

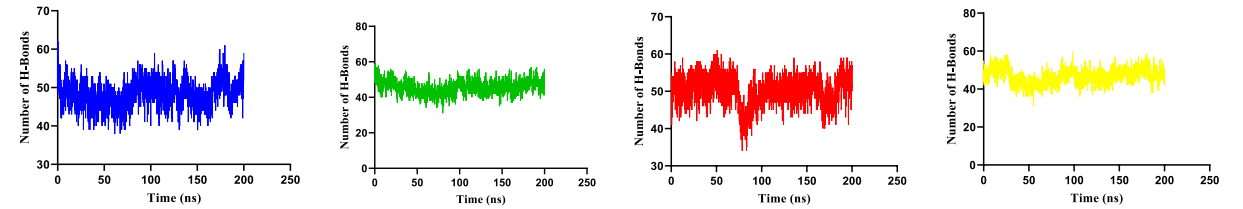

Fig. 18. H-bond of **(blue)** LMP-1, **(green)** Chlorogenic acid, **(red)** EGCG, and **(yellow)** Isoquercetin.

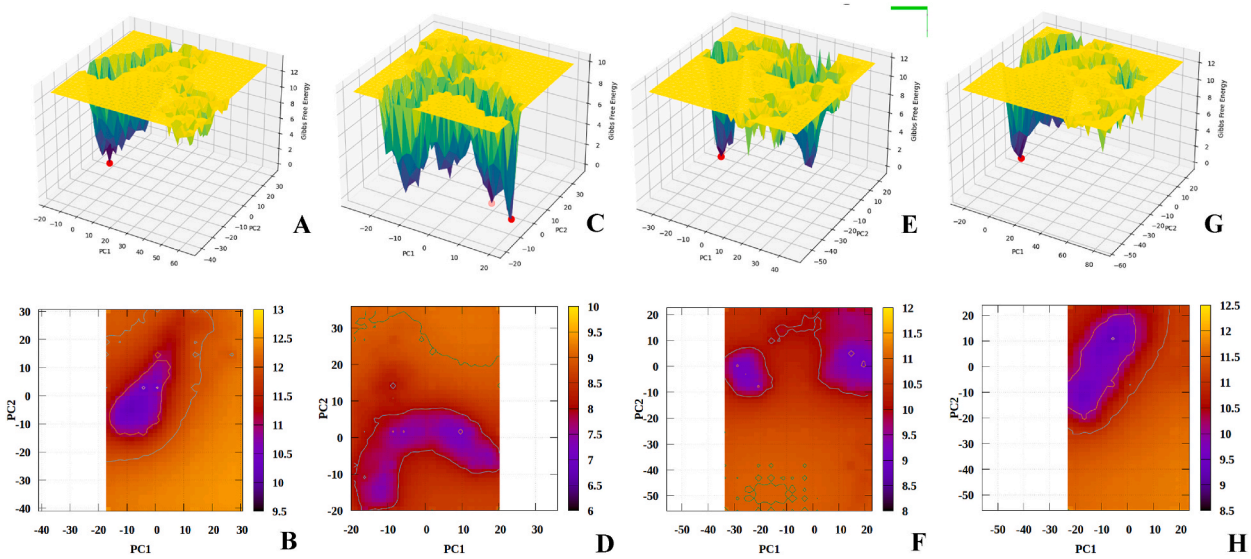

Fig. 19. Free energy landscape with minima for **A, B)** EBNA-1 **C, D)** Chlorogenic acid **E, F)** EGCG and **G, H)** Isoquercetin.

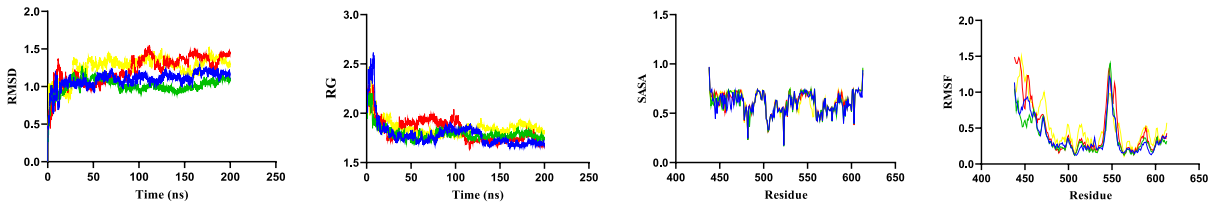

Fig. 20. MD analysis of **(blue)** EBNA-1, **(green)** Chlorogenic acid, **(red)** EGCG, and **(yellow)** Isoquercetin.

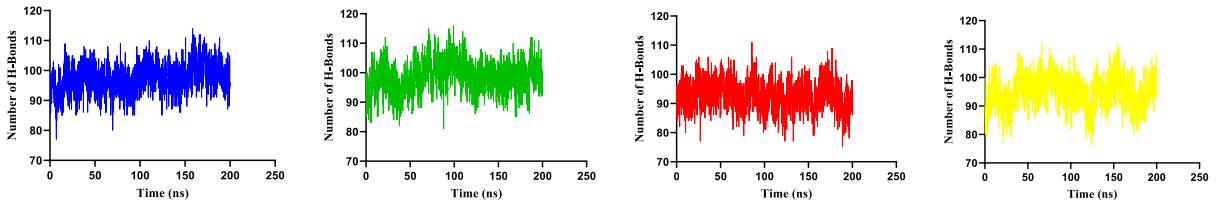

Fig. 21. H-bond of **(blue)** EBNA-1, **(green)** Chlorogenic acid, **(red)** EGCG, and **(yellow)** Isoquercetin.

functionally effective active site. Chlorogenic Acid also induces some compactness, but the effect is weaker compared to EGCG. It results in a moderately compact conformation. Isoquercetin has the least effect on the compactness of EBNA1, which is reflected in a larger RG value. This indicates that the ligand induces a more open and less stable conformation in the protein. EGCG significantly reduces the SASA of the active site, which indicates that it effectively blocks solvent access to the active site. This reduction in solvent exposure suggests that EGCG stabilizes the protein and prevents other molecules from interacting with the active site. Chlorogenic acid also reduces the SASA, but not as effectively as EGCG. This leads to moderate stabilization of the active site. Isoquercetin results in the least reduction of SASA, which correlates with its lower efficacy in inhibiting EBNA1 (see Fig. 21).

4. Conclusion

Having antioxidant properties, these compounds can prevent the spread of diseases by inhibiting free radicals and oxidative stress, and if nanoparticles of these compounds are used, their antioxidant properties can be increased. Also, the results of the green synthesis of gold nanoparticles by saffron extract and its investigation showed that this is a suitable reducing agent for the preparation of gold nanoparticles by the green method. The resulting nanoparticles showed spherical and triangular shapes and very good dispersion in the

distribution of nanoparticles. The chemical compounds in saffron aqueous extract are effective in inhibiting destructive and inflammatory proteins. Molecular docking and dynamic show quercetin exhibit the best inhibitory effect on MMP9 due to its ability to stabilize the active site, reduce fluctuations, and form strong hydrogen bonds. In addition, among the tested ligands, HTCC showed the most significant effect on the active site of TNF. It strongly stabilized the active site residues. It minimized conformational fluctuations (as shown by low RMSF values). It formed a robust network of interactions, particularly with critical residues like Arg, Glu, and Tyr. Finally, EGCG is the most promising ligand due to its ability to form strong interactions with the active site residues and reduce flexibility, leading to effective inhibition of LMP1. Also, EGCG is the most promising candidate for EBNA1 inhibition. It induces structural stability, reduces flexibility, and enhances protein compactness, making it the most effective ligand.

CRediT authorship contribution statement

Shaghayegh Mohammadi: Writing – original draft, Software, Methodology, Investigation. **Hamed Farjam:** Writing – review & editing, Software, Investigation. **Sharieh Hosseini:** Writing – original draft, Supervision. **Kambiz Larijani:** Writing – review & editing, Validation.

Data availability statement

All data are available in the manuscript text.

Declaration of competing interest

The authors declare that they have no known competing financial interests or personal relationships that could have appeared to influence the work reported in this paper.

References

[1] R. Srivastava, H. Ahmed, R. Dixit, Dharamveer, S. Saraf, "Crocus sativus L.: a comprehensive review,", Pharmacogn. Rev. 4 (8) (2010) 200–208, https://doi.org/10.4103/0973-7847.70919.
[2] A. Zhang, et al., Polysaccharide and crocin contents, and antioxidant activity of saffron from different origins, Ind. Crops Prod. 133 (November 2018) (2019) 111–117, https://doi.org/10.1016/j.indcrop.2019.03.009.
[3] M. José Bagur, et al., Saffron: an Old medicinal plant and a potential novel functional food, Molecules 23 (1) (2017) 1–21, https://doi.org/10.3390/molecules23010030.
[4] H. Ashktorab, et al., Saffron : the golden spice with therapeutic, Nutrients 11 (2019) 1–16.
[5] L. Cardone, D. Castronuovo, M. Perniola, N. Cicco, V. Candido, Saffron (Crocus sativus L.), the king of spices: an overview, Sci. Hortic. (Amst.) 272 (February) (2020), https://doi.org/10.1016/j.scienta.2020.109560.
[6] A.M. Deslauriers, et al., Neuroinflammation and endoplasmic reticulum stress are coregulated by crocin to prevent demyelination and neurodegeneration, J. Immunol. 187 (9) (2011) 4788–4799, https://doi.org/10.4049/jimmunol.1004111.
[7] S. Soeda, T. Ochiai, L. Paopong, H. Tanaka, Y. Shoyama, H. Shimeno, Crocin suppresses tumor necrosis factor-α-induced cell death of neuronally differentiated PC-12 cells, Life Sci. 69 (24) (2001) 2887–2898, https://doi.org/10.1016/S0024-3205(01)01357-1.
[8] C. Orabona, et al., Crocus sativus L. Petal extract inhibits inflammation and osteoclastogenesis in RAW 264.7 cell model, Pharmaceutics 14 (6) (2022), https://doi.org/10.3390/pharmaceutics14061290.
[9] S. Samarghandian, A. Borji, Anticarcinogenic effect of saffron (Crocus sativus L.) and its ingredients, Pharmacogn. Res. 6 (2) (2014) 99–107, https://doi.org/10.4103/0974-8490.128963.
[10] A.U. Mirza, et al., Biomediated synthesis, characterization, and biological applications of nickel oxide nanoparticles derived from Toona ciliata, Ficus carica and Pinus roxburghii, Bioproc. Biosyst. Eng. 44 (7) (2021) 1461–1476, https://doi.org/10.1007/s00449-021-02528-4.
[11] N.A. Begum, S. Mondal, S. Basu, R.A. Laskar, D. Mandal, Biogenic synthesis of Au and Ag nanoparticles using aqueous solutions of Black Tea leaf extracts, Colloids Surf. B Biointerfaces 71 (1) (2009) 113–118, https://doi.org/10.1016/j.colsurfb.2009.01.012.
[12] A. Oukarroum, S. Bras, F. Perreault, R. Popovic, Inhibitory effects of silver nanoparticles in two green algae, Chlorella vulgaris and Dunaliella tertiolecta, Ecotoxicol. Environ. Saf. 78 (Apr. 2012) 80–85, https://doi.org/10.1016/j.ecoenv.2011.11.012.
[13] M. Parveen, et al., Comparative study of biogenically synthesized silver and gold nanoparticles of Acacia auriculiformis leaves and their efficacy against Alzheimer's and Parkinson's disease, Int. J. Biol. Macromol. 203 (Apr. 2022) 292–301, https://doi.org/10.1016/j.ijbiomac.2022.01.116.
[14] P. Dauthal, M. Mukhopadhyay, Noble metal nanoparticles: plant-mediated synthesis, mechanistic aspects of synthesis, and applications, Ind. Eng. Chem. Res. 55 (36) (2016) 9557–9577, https://doi.org/10.1021/acs.iecr.6b00861.
[15] K.X. Lee, et al., Recent developments in the facile bio-synthesis of gold nanoparticles (AuNPs) and their biomedical applications, Int. J. Nanomed. 15 (2020) 275–300, https://doi.org/10.2147/IJN.S233789.
[16] W. Li, et al., AuNPs as an important inorganic nanoparticle applied in drug carrier systems, Artif. Cells, Nanomed. Biotechnol. 47 (1) (2019) 4222–4233, https://doi.org/10.1080/21691401.2019.1687501.
[17] N. Sharma, G. Bhatt, P. Kothiyal, Gold Nanoparticles synthesis, properties, and forthcoming applications : a review, Indian J. Pharmaceut. Biol. Res. 3 (2) (2015) 13–27, https://doi.org/10.30750/ijpbr.3.2.3.
[18] S. Ahmed, Annu S. Ikram, S. Yudha, Biosynthesis of gold nanoparticles: a green approach, J. Photochem. Photobiol. B Biol. 161 (2016) 141–153, https://doi.org/10.1016/j.jphotobiol.2016.04.034.
[19] M. Hassanisaadi, G.H.S. Bonjar, A. Rahdar, S. Pandey, A. Hosseinipour, R. Abdolshahi, Environmentally safe biosynthesis of gold nanoparticles using plant water extracts, Nanomaterials 11 (8) (2021), https://doi.org/10.3390/nano11082033.
[20] H. seok Kim, Y.S. Seo, K. Kim, J.W. Han, Y. Park, S. Cho, Concentration effect of reducing agents on green synthesis of gold nanoparticles: size, morphology, and growth mechanism, Nanoscale Res. Lett. 11 (1) (2016), https://doi.org/10.1186/s11671-016-1393-x.
[21] D. Zhang, X. Ma, Y. Gu, H. Huang, G. Zhang, Green synthesis of metallic nanoparticles and their potential applications to treat cancer 8 (October) (2020) 1–18, https://doi.org/10.3389/fchem.2020.00799.
[22] G. Kobelt, A. Thompson, J. Berg, M. Gannedahl, J. Eriksson, New insights into the burden and costs of multiple sclerosis in Europe, Mult. Scler. 23 (8) (2017) 1123–1136, https://doi.org/10.1177/1352458517694432.
[23] R. Dobson, G. Giovannoni, Multiple sclerosis – a review, Eur. J. Neurol. 26 (1) (2019) 27–40, https://doi.org/10.1111/ene.13819.
[24] A.L. Greenfield, S.L. Hauser, B-Cell therapy for multiple sclerosis: entering an era, Ann. Neurol. 83 (1) (2018) 13–26, https://doi.org/10.1002/ana.25119.

[25] A.J. Coles, et al., The window of therapeutic opportunity in multiple sclerosis: evidence from monoclonal antibody therapy, J. Neurol. 253 (1) (2006) 98–108, https://doi.org/10.1007/s00415-005-0934-5.
[26] E. Leray, et al., Evidence for a two-stage disability progression in multiple sclerosis, Brain 133 (7) (2010) 1900–1913, https://doi.org/10.1093/brain/awq076.
[27] K. Peter, Christopher, M. Murtaugh, "Association between tumor necrosis factor-α and disease progression, in: Patients with Multiple Sclerosis,", 1999.
[28] P14780 · MMP9_HUMAN." [Online]. Available: https://www.uniprot.org/uniprotkb/P14780/entry.
[29] F.G. Sakha, A.A. Saeen, S.M. Moazzeni, F. Etesam, G. Vaezi, A randomized, triple-blind placebo-controlled trial to determine the effect of saffron on the serum levels of MMP-9 and TIMP-1 in patients with multiple sclerosis, Iran J Allergy Asthma Immunol 19 (3) (2020) 297–304, https://doi.org/10.18502/ijaai.v19i3.3457.
[30] L. Jiang, et al., EBNA1-targeted inhibitors: novel approaches for the treatment of Epstein-Barr virus-associated cancers, Theranostics 8 (19) (2018) 5307–5319, https://doi.org/10.7150/thno.26823.
[31] Lymphocryptovirus." [Online]. Available: https://viralzone.expasy.org/185.
[32] J.M.D. James, C. Niederman, Miller George, Howard A. Pearson, Joseph S. Pagano, Infectious mononucleosis Epstein-Barr-Virus shedding in salvia and the Oropharynx, N. Engl. J. Med. 294 (25) (1976) 327–329.
[33] D.R. Rawlins, G. Milman, S.D. Hayward, G.S. Hayward, Sequence-specific DNA binding of the Epstein-Barr virus nuclear antigen (EBNA-1) to clustered sites in the plasmid maintenance region, Cell 42 (3) (1985) 859–868, https://doi.org/10.1016/0092-8674(85)90282-X.
[34] J. Sears, M. Ujihara, S. Wong, C. Ott, J. Middeldorp, A. Aiyar, The amino terminus of epstein-Barr virus (EBV) nuclear antigen 1 contains AT hooks that facilitate the replication and partitioning of latent EBV genomes by tethering them to cellular chromosomes, J. Virol. 78 (21) (2004) 11487–11505, https://doi.org/10.1128/jvi.78.21.11487-11505.2004.
[35] "P03211 · EBNA1_EBVB9." [Online]. Available: https://www.uniprot.org/uniprotkb/P03211/entry.
[36] H. Summers, J.A. Barwell, R.A. Pfuetzner, A.M. Edwards, L. Frappier, Cooperative assembly of EBNA1 on the Epstein-Barr virus latent origin of replication, J. Virol. 70 (2) (1996) 1228–1231, https://doi.org/10.1128/jvi.70.2.1228-1231.1996.
[37] Z.K. Taravat Khodaei, Jhamak Nourmohammadi, Azadeh Ghaee, An antibacterial and self-healing hydrogel from aldehyde-carrageenan for wound healing applications, Carbohydr. Polym. 302 (2023), https://doi.org/10.1016/j.carbpol.2022.120371.
[38] J.C. Johan van Meerloo, Gertjan J.L. Kaspers, Cell sensitivity assays: the MTT assay Johan, Cancer Cell Cult 731 (2003) 237–245, https://doi.org/10.1385/1592594069.
[39] M. Ruggieri, et al., Effect of cladribine on neuronal apoptosis: new insight of in vitro study in multiple sclerosis therapy, Brain Sci. 10 (8) (2020) 1–13, https://doi.org/10.3390/brainsci10080548.
[40] M. Bertoni, F. Kiefer, M. Biasini, L. Bordoli, T. Schwede, Modeling protein quaternary structure of homo- and hetero-oligomers beyond binary interactions by homology, Sci. Rep. 7 (1) (2017) 1–15, https://doi.org/10.1038/s41598-017-09654-8.
[41] N. Guex, M.C. Peitsch, T. Schwede, Automated comparative protein structure modeling with SWISS-MODEL and Swiss-PdbViewer: a historical perspective, Electrophoresis 30 (1) (2009) 162–173, https://doi.org/10.1002/elps.200900140.
[42] N. Guex, M.C. Peitsch, SWISS-MODEL and the Swiss-PdbViewer: an environment for comparative protein modeling, Electrophoresis 18 (15) (1997) 2714–2723, https://doi.org/10.1002/elps.1150181505.
[43] M.U. Johansson, V. Zoete, O. Michielin, N. Guex, Defining and searching for structural motifs using DeepView/Swiss-PdbViewer, BMC Bioinf. 13 (1) (2012), https://doi.org/10.1186/1471-2105-13-173.
[44] T. Schwede, J. Kopp, N. Guex, M.C. Peitsch, SWISS-MODEL: an automated protein homology-modeling server, Nucleic Acids Res. 31 (13) (2003) 3381–3385, https://doi.org/10.1093/nar/gkg520.